Electrochemical Promotion by Sodium of the Rhodium-Catalyzed NO + CO Reaction

Federico J. Williams, Alejandra Palermo, Mintcho S. Tikhov, and Richard M. Lambert*

Department of Chemistry, University of Cambridge, Cambridge CB2 1EW, U.K.

Received: May 4, 2000

XPS shows that the electropumping of Na to a metallic Rh film contacted with a solid electrolyte (Na β'' alumina) under potentiostatic conditions results in reversible spillover of the alkali from the electrolyte to the catalytically active surface. As the catalyst potential (V_{WR}) is decreased over a range of 2000 mV, the sodium coverage increases linearly from zero to ~0.02 monolayers, while the work function (ϕ) decreases, also linearly, by 0.65 eV. Over this same regime of catalyst potential, under approximately stoichiometric conditions, both the activity and N_2 selectivity of the NO + CO reaction are strongly enhanced as Na is pumped to the Rh surface. The measured Na coverage, electrochemical behavior, and catalytic response of the system are fully reversible with catalyst potential. Our data are understandable in terms of the Na-induced dissociation of adsorbed NO, which is thought to be the rate-limiting step. The nature of electrochemical promotion, the reaction mechanism, the mode of promoter action, and the inequivalence of $\Delta\phi$ and ΔV_{WR} are discussed.

1. Introduction

The metal-catalyzed heterogeneous reduction of CO by NO serves as a paradigm in catalytic science. It has been investigated over many years under a wide range of conditions and by means of a variety of catalyst types, including single crystals, polycrystalline foils and wires, and oxide-supported metals. The earliest study carried out on single-crystal surfaces under ultrahigh vacuum conditions was that of Lambert and Comrie,[1] who examined the reaction on Pt{111} and Pt{110}. More recently, Zaera et al.[2] and Belton et al.[3] have investigated the reaction on single-crystal surfaces of rhodium using molecular beam techniques and atmospheric pressure conditions, respectively. The motivation for much current work on this topic derives, at least in part, from the important role played by the CO + NO reaction in practical automotive catalytic converters;[4] our recent contributions to this subject have involved the application of alkali promotion using both electrochemical and classical methods, as indicated below.

We have shown that on Pt surfaces promotion by (electrochemically supplied) Na greatly enhances both activity and selectivity toward N_2 production in the CO + NO reaction.[5] A mechanistic model was proposed and subsequently supported by Monte Carlo calculations.[6] This work eventually led to the development of highly active and selective alkali-promoted Pd and Pt dispersed catalysts.[7,8] Most recently, we have shown that Pt/γ−alumina-dispersed catalysts exhibit strong promotion by Na under simulated exhaust gas conditions.[9]

As we have shown, the efficacy of alkalis in promoting activity and selectivity in NO reduction over Pt and Pd derives from alkali-induced NO dissociation on these metal surfaces, which otherwise are not very efficient for NO dissociation. In this respect, clean Rh surfaces are much more efficient than both Pt and Pd surfaces, and this indeed is why Rh is a vital component in automotive catalytic converters. However, the mechanism of Rh-catalyzed NO reduction by CO remains controversial.

The present work is principally motivated by the following questions. Can the catalytic performance of Rh be usefully enhanced by alkali promotion? What can alkali promotion reveal about the reaction mechanism? In addition, we address some fundamental issues of electrochemical promotion (EP). EP provides in situ control of promoter concentration at the surface of a working metal catalyst.[10] This is achieved by pumping promoter species (Na in the present case) to or from a suitable solid electrolyte (Na β'' alumina in the present case) to a porous metal film catalyst with which it is in contact. By varying the catalyst potential with respect to a reference electrode (potentiostatic control), we may reverse the alkali coverage, work function, and catalytic behavior of the metal surface. The relationship between catalyst potential, work function, and alkali coverage is of fundamental interest, and we investigate this. We find that alkali promotion is effective in enhancing the catalytic performance of Rh and the data point to NO dissociation as the rate-limiting step.

2. Experimental Methods

2.1. Apparatus. UPS and XPS experiments were performed under UHV conditions (base pressure, $<10^{-10}$ Torr) in a VG ADES 400 UHV spectrometer system equipped with a reaction cell. The EP sample was mounted on a manipulator that allowed translation between the reaction cell and the spectrometer chamber. Full details regarding sample mounting, manipulation, and data acquisition are given in an earlier publication.[10] Quoted binding energies are referred to the Au4f$_{7/2}$ emission at 83.8 eV from the Au wire that formed the electrical connection to the Rh working electrode. Work function changes were determined by measuring the change in secondary electron cutoff in the UP spectrum relative to the Fermi edge.

Reactor measurements were performed in a well-mixed reactor operated at atmospheric pressure. The EP sample was suspended in this reactor with all electrodes exposed to the reactant gas mixture. Inlet and exit gas analysis was carried out by a combination of on-line gas chromatography (Shimadzu-14B; molecular sieve 13X and Haysep-N columns) and on-line

* Corresponding author. Tel: 44 1223 336467. Fax: 44 1223 336362. Email: RML1@cam.ac.uk.

10.1021/jp001689x CCC: $19.00
Published on Web 11/30/2000

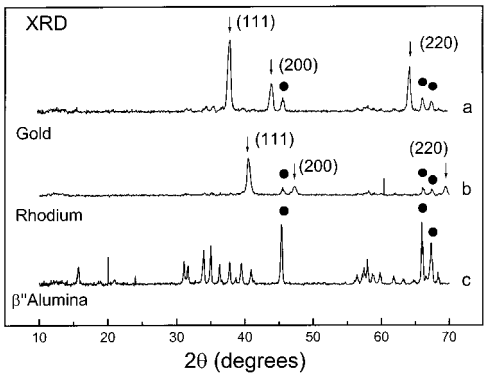

Figure 1. XRD patterns from (a) the bare Na β''alumina wafer, (b) the Rh film subsequently deposited on one face, and (c) the gold film deposited on the other face.

mass spectrometry (Balzers QMG 064). N_2, N_2O, CO, and CO_2 were measured by gas chromatography, and NO was monitored continuously by mass spectrometry after the necessary calibrations were performed. NO (Distillers MG) and CO (Distillers MG) were diluted in ultrapure He (99.996%) and fed to the reactor by mass flow controllers (Brooks 5850 TR). The total flow rate was kept constant in all experiments at 34×10^{-5} mol s^{-1} (500 cm^3(STP)/min), with partial pressures P_{NO} and P_{CO} of 0.2−1.8 and 0.3−1.1 kPa, respectively, with added helium (P_{He}) giving a total pressure of 1 atm in every case. Reactant conversion was restricted to <15% in order to avoid mass transfer limitations. Control experiments were carried out in which the total flow was varied by a factor of 5 in order to verify that the observed changes in activity were indeed due to changes in actual surface reaction rates and unaffected by mass transfer limitations. Nitrogen and carbon mass balances always closed to within 5%.

A galvanostat-potentiostat (Ionic Systems) was used in order to maintain a given potential difference between the working and reference electrodes (potentiostatic mode). All experiments were carried out in potentiostatic mode by following the effect of catalyst potential (V_{WR}, measured with respect to the reference electrode) on (i) the sodium coverage (UPS/XPS experiments) and (ii) the reaction rates (CSTR experiments). In a separate control experiment, the ohmic drop free potential of the working electrode was determined using the current interruption technique. Current interruption was achieved by means of an analogue switch (ADG201HS) with a response time of 50 ns. A digital oscilloscope was use to record the ohmic drop. The results showed that the ohmic drop contribution to V_{WR} could be neglected under all conditions. That is, the V_{WR} values reported below are true values. XRD data were obtained on a Philips PW1877 automated powder diffractometer, using a Cu Kα source (λ = 1.540 56 Å). All spectra were taken over a range of $10° < 2\theta < 70°$ and referenced to the JCPDS database.

2.2. Sample Preparation and Characterization. The EP samples for spectroscopic examination and catalytic testing were prepared by depositing a rhodium metal film on one face of a Na-β'' alumina wafer: this constituted the catalyst (working electrode). The gold counter and reference electrodes were deposited on the other face, all three electrodes being deposited by DC sputtering of Rh or Au in argon. The wafer dimensions were 2 cm × 2 cm × 0.1 cm (spectroscopy) and 1 cm × 0.3 cm × 0.1 cm (catalytic testing), the latter being determined by the need to limit reactant conversion to <15%.

These EP samples were characterized by XRD, XPS, and surface area measurements. Figure 1 shows the XRD patterns from (i) the bare Na β''alumina wafer, (ii) the Rh film deposited on one face, and (iii) the gold film deposited on the other face. The rhodium and gold patterns show three peaks characteristic of the relevant metal (arrowed) and three additional peaks due to the underlying β''alumina (filled circle).

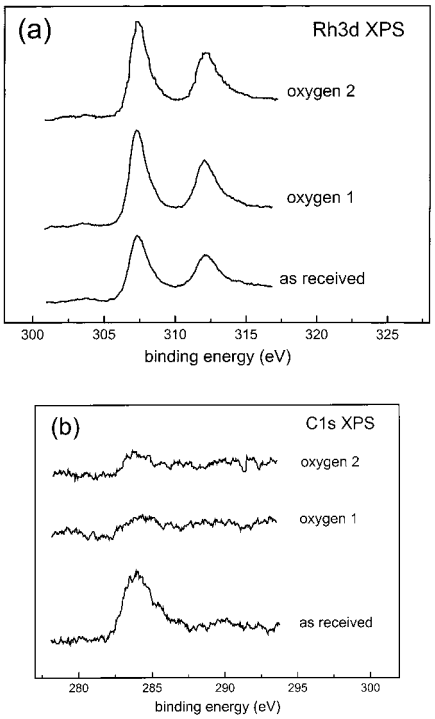

Figure 2. XP spectra showing the effect of oxygen pretreatments on the amount of carbon on the catalyst. (a) Rh 3d spectra and (b) C 1s spectra.

The bottom spectra in Figure 2a,b correspond to the Rh 3d and C 1s XP spectra of the EP sample immediately after installation. The binding energies indicate that the film consisted of metallic rhodium (Rh $3d_{5/2}$ at 307.3 eV) and that the only observable impurity was elemental carbon (C 1s at 284 eV). To remove the carbon, we treated the sample with oxygen in the reaction cell (P_{O2} = 0.2 mbar at T = 563K and V_{WR} = +1000 mV for 15 min). The spectra resulting from two successive oxygen treatments are shown in Figure 2a,b. Cleaning the rhodium film with oxygen resulted in a 37% increase of the Rh signal and a 81% decrease in the carbon signal, with no detectable oxidation of the rhodium surface.

The active metal area of the rhodium catalyst was determined using two different methods: (i) the CO methanation technique developed by Komai et al.[11] and (ii) the electrochemical technique developed by Vayenas et al.[12] (Before measuring the surface area, we calcined the sample in oxygen and reduced it with hydrogen at 573 K in order to generate a clean metal surface.) The first method makes use of a sensitive FID detector to monitor the conversion of chemisorbed CO to methane on metal sites. On the basis of a 1:1 CO-to-surface-metal atom ratio, this yields a surface area equivalent to 1.5 μmol Rh (~560 cm^2). The second technique involves measuring galvanostatic transients. A fixed negative current was applied between the working and counter electrodes (i.e., sodium supply to the catalyst) while measuring the resulting changes in catalyst potential as a function of time. It can be shown using Faraday's Law and the Helmholz equation[12] that

$$A = \frac{P_0 I}{\epsilon_0 \frac{d\phi}{dt}} \quad (1)$$

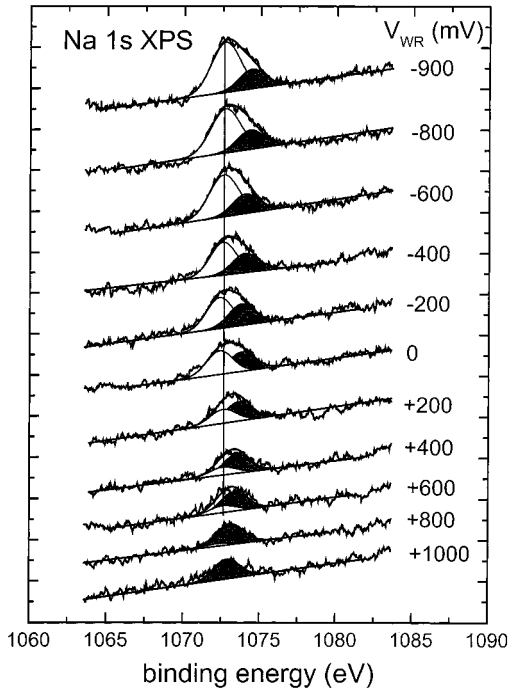

Figure 3. Na 1s XPS spectra showing the effect of catalyst potential on the sodium coverage of the Rh film under UHV conditions at 580 K. Invariant component due to Na on Rh; shifting component due to Na in solid electrolyte.

where A is the catalyst surface area (m^2), P_0 is the initial dipole moment of Na on Rh (1.7×10^{-29} C m^{13}), $I = -10 \times 10^{-6}$ C/s is the constant current applied between the working and counter electrodes, $\epsilon_0 = 8.85 \times 10^{-12}$ C^2/J m, and $d\phi/dt$ is the initial slope of the work function versus time curve. As we cannot determine $d\phi/dt$ experimentally, we measured edV_{WR}/dt and used the relationship between edV_{WR} and $d\phi$ (discussed below); thus, $edV_{WR}/dt = -1.12 \times 10^{-21}$ J/s, and $d\phi = 0.32edV_{WR}$. Inserting these values in eq 1 yields a surface area of ~552 cm^2 (using a surface metal atom density of 1.6×10^{15} atom/cm^2, which corresponds to the {111} plane of Rh). This is equivalent to 1.4 μmol Rh, in good agreement with the value measured by CO methanation (1.5 μmol Rh). In a similar fashion, the metal surface area of the sample used for the reactor measurements was found to be equivalent to 0.1 μmol Rh, or ~37.6 cm^2.

3. Results

3.1. Photoelectron Spectroscopies. Figure 3 shows Na 1s XP spectra obtained at 580 K as a function of catalyst potential (V_{WR}) under ultrahigh vacuum conditions. The +1000 mV spectrum corresponds to the electrochemically cleaned sample; increasingly negative values of V_{WR} correspond to increasing amounts of electropumped Na on the catalyst surface. These observations confirm that EP works by supplying alkali promoter species to the catalyst surface. The spectral behavior was reversible and reproducible as a function of V_{WR}, consistent with the reversible and reproducible catalytic response under reaction conditions at atmospheric pressure (see below). Note the residual Na 1s emission from the electrochemically cleaned sample. To understand this, recall that the rhodium film is both thin and porous. The Na 1s emission therefore comprises two components, one due to the Na present on the surface of the Rh film, the other due to Na present in the underlying β''alumina electrolyte which was visible to XPS through the cracks and pores in the metal film. The component due to the Na on the

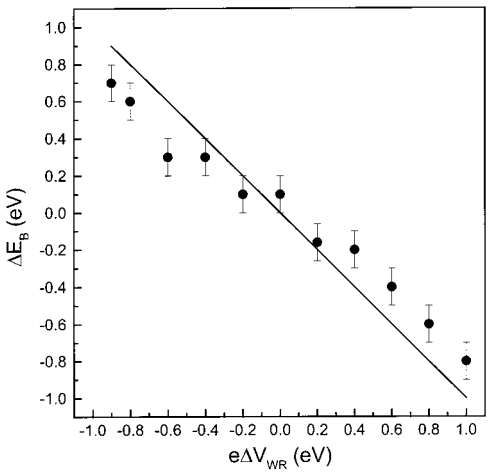

Figure 4. Binding energy shift of the Na 1s XPS component due to Na in the solid electrolyte as a function of the change in V_{WR}.

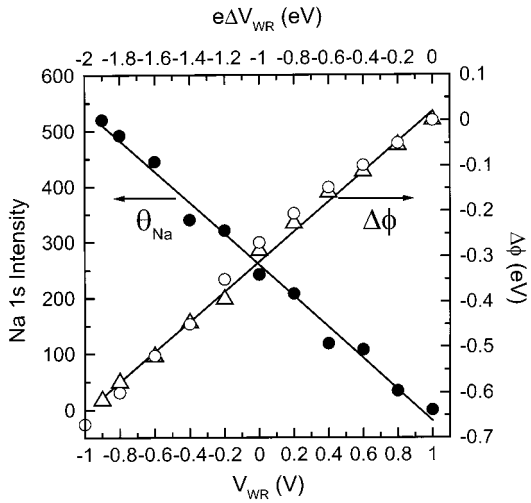

Figure 5. Integrated Na 1s XPS intensity due to sodium on the rhodium surface and associated work function change of the rhodium film as a function of catalyst potential.

Rh catalyst exhibits invariant binding energy (BE) and increases in intensity with decreasing V_{WR}. In contrast with this, the other component exhibits constant intensity and a systematic shift in apparent BE (ΔE_B). This shift is numerically equal to the change in V_{WR}, as shown in Figure 4, where the apparent binding energy shift of the Na component ascribed to the Na β''alumina has been plotted against ΔV_{WR}. These results confirm that this component of the Na 1s emission arises from the solid electrolyte whose electrostatic potential differs from that of the Rh film by the amount ΔV_{WR}.

The filled circles in Figure 5 show the integrated Na 1s emission intensity versus V_{WR}. For $V_{WR} <$ ~1000 mV, decreasing the catalyst potential causes a linear increase of the sodium coverage with potential. It is significant that over this same regime, the work function also varies linearly with V_{WR} (see Figure 5 and below). A value for the sodium coverage (ϑ_{Na}) may be estimated from the integrated Na 1s intensity of the component associated with the Rh surface by making use of the relationship derived by Carley et al[14]

$$\vartheta_{Na} = \frac{Y_m \sigma_s N \rho \lambda \cos \psi}{Y_s \sigma_m M_s} \quad (2)$$

where Y_m is the integrated photoelectron signal from a particular subshell of the adatom (i.e., Na(1s)); Y_s is the integrated signal

from the relevant subshell of the substrate (i.e., Rh(3d)), σ_m and σ_s are the subshell photoionization cross sections for the adatom and the substrate, respectively, M_s is the relative atomic mass of the substrate, ρ is the density of the substrate, λ is the escape depth in the substrate for the substrate photoelectrons, ψ is the angle of detection with respect to the sample normal of the photoelectrons, and N is Avogadro's number. The subshell photoionization cross sections and escape depth have been taken from the calculations of Yeh et al.[15] and Penn,[16] respectively.

On this basis, the highest Na coverage achieved ($V_{WR} = -900$ mV, Figure 3) corresponds to 2.84×10^{15} atom/cm^2, equivalent to ~1.7 monolayers (ML), where 1 ML is defined as one sodium adatom per substrate atom. Such a coverage of sodium should attenuate the Rh 3d XPS signal by ~50% relative to that from the sodium free surface; however, no such attenuation was observed. The reason for this apparent discrepancy is that eq 2 is valid for an ideally flat substrate, whereas our samples are very rough. Thus, eq 2 gives an overestimate of the actual sodium coverage because the true metal surface area is much greater than the geometrical area of the Rh film. We may take this roughness factor into account in order to produce a more realistic estimate of the sodium coverage by applying a simple correction factor to the right-hand side of eq 2. This factor is just the geometrical surface area divided by the true metal area. The resulting calculated sodium coverage at $V_{WR} = -900$ mV is then 0.013 ML, in good agreement with the observed lack of attenuation of the Rh XPS intensity. It is also in good accord with the linear dependence of the work function on sodium coverage, as discussed below.

Work function data provide complementary information about the surface processes occurring during the spillover of electropumped Na. In Figure 5, the open circles show the work function change ($\Delta\phi$) when the catalyst potential is systematically decreased from +1000 to −1000 mV at 580 K; the open triangles show the corresponding data obtained when the process was reversed, i.e., when the catalyst potential was increased from −1000 to +1000 mV. Thus, the value of $\Delta\phi$ corresponding to a particular value of V_{WR} is independent of the sample history. This indicates that (i) the spillover process is reversible and (ii) a given V_{WR} corresponds to a given sodium coverage.

It is apparent from Figure 5 that $\Delta\phi$ varies linearly with both catalyst potential and ϑ_{Na}. This is a clear indication that we are in the low alkali coverage regime, where such behavior is to be expected.[17] Specifically, ϑ_{Na} must be less than ~0.1 ML.[13] The maximum sodium coverage achieved in the experiments whose results are illustrated in Figure 5 caused a work function decrease of −0.65 eV. Comparison with single-crystal data obtained for the Rh(111)/Na system[13] indicates that in the present case, $V_{WR} = -900$ mV corresponds to ϑ_{Na} ~0.025 ML, i.e., about twice the value based on XPS intensity analysis. This is a satisfactory level of agreement. For present purposes, they key point is that two independent methods indicate that our experimental data span the range of $0 < \vartheta_{Na} < \sim 0.02$.

We now describe the catalytic consequences of Na pumping to the Rh surface.

3.2. Effect of Catalyst Potential on Reaction Rates. Figure 6 shows typical steady-state (potentiostatic) rate data obtained at 1 atm pressure and 580 K for constant inlet pressures of NO and CO, $P^0_{CO} = P^0_{NO} = 1$ kPa. Turnover frequencies (TOF) are expressed as molecules of product per Rh surface atom per second. It is apparent that the CO_2, N_2O, and N_2 turnover frequencies are dependent on the catalyst potential, and the observed behavior was fully reversible with V_{WR}. Also shown

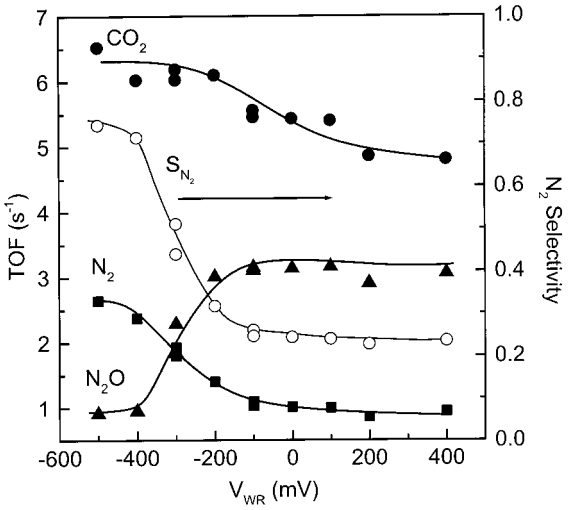

Figure 6. Effect of catalyst potential (V_{WR}) on the CO_2, N_2, and N_2O formation rates and the nitrogen selectivity. Conditions: $T = 580$ K, $P^0_{NO} = P^0_{CO} = 1$ kPa.

in Figure 6 is the dependence of N_2 selectivity on V_{WR}, where the former quantity is defined as

$$S_{N_2} = \frac{r_{N_2}}{r_{N_2} + r_{N_2O}} \tag{3}$$

These data show that the rates of CO_2 and N_2 production increase with decreasing V_{WR}, whereas the N_2O rate decreases. Thus, the system exhibits pronounced electrochemical promotion: Na induces an increase in overall activity and in N_2 production at the expense of N_2O production, resulting in an increase in nitrogen selectivity from 24% to 80%. The rate enhancement ratios (ρ) defined as the ratio of the maximum promoted rates to the unpromoted rates are as follows: $\rho(CO_2) = 1.4$, $\rho(N_2) = 3.1$, and $\rho(N_2O) = 0.3$. The observed changes in turnover frequencies and nitrogen selectivity were fully reversible; i.e., returning V_{WR} to the initial value restored all the reaction rates to their initial values. It is worth noting that our TOF values for the unpromoted Rh film are very similar to those reported for the CO + NO reaction over Rh(111) under similar conditions of temperature and reactant pressures.[18,19] This provides additional validation for our estimate of the surface area of the rhodium film.

3.3. Effect of Reactant Partial Pressures on Promoted and Unpromoted Reaction Rates. The dependence of the CO_2, N_2, and N_2O reaction rates on P_{CO} at fixed P_{NO} for three different values of catalyst potential is illustrated in Figure 7a−c. $V_{WR} = +200$ mV corresponds to the clean Rh surface (unpromoted rate), while $V_{WR} = -200$ mV and $V_{WR} = -400$ mV correspond to promoted surfaces with progressively increased sodium loadings. Figure 7d shows the corresponding nitrogen selectivity data: it is apparent that the highest selectivities to nitrogen production always occur in the presence of the highest Na loading (most negative potential). From Figure 7a,b it can be seen that the CO_2 and N_2 rates exhibit Langmuir−Hinshelwood behavior and that increased levels of Na result in a small systematic increase in the CO partial pressure (P^*_{CO}) necessary for inhibition. That is, Na favors the chemisorption of NO relative to that of CO. The N_2O rate also exhibits Langmuir−Hinshelwood kinetics, but the effect of increased Na is somewhat different: in particular, high levels of Na suppress the N_2O rate, and there is no systematic shift in P^*_{CO}. Thus increasing the sodium coverage causes an increase in the rates

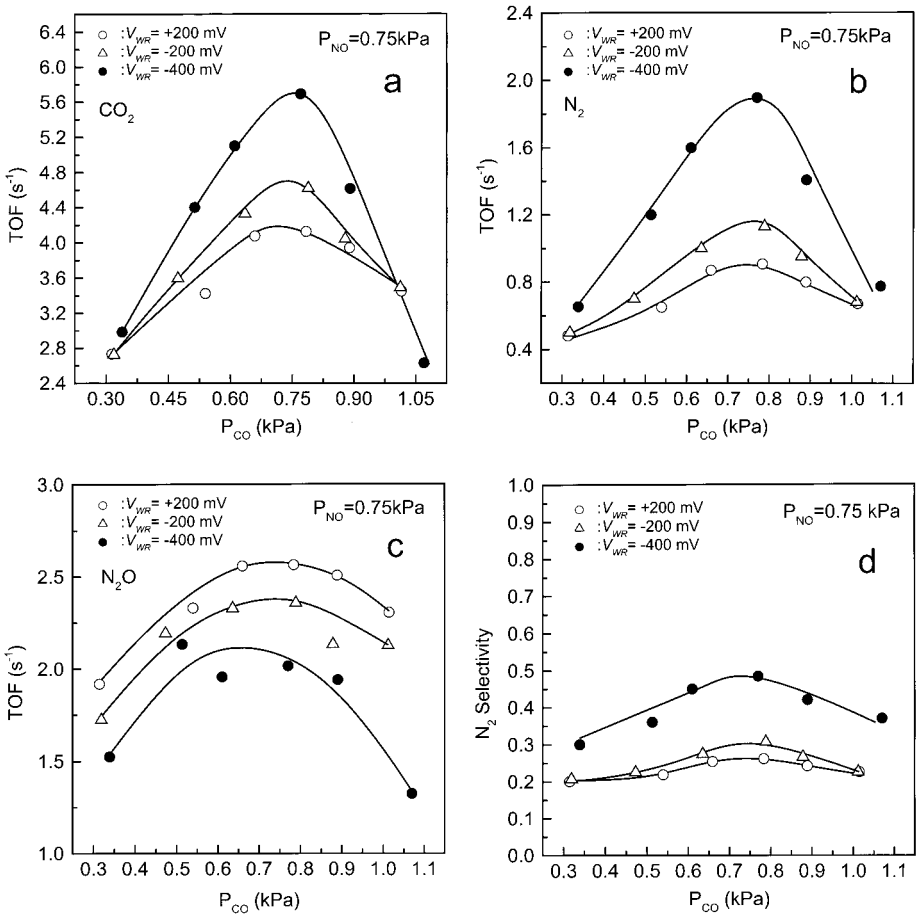

Figure 7. Effect of the partial pressure of CO (P_{CO}) on the rates of CO_2 (a), N_2 (b), and N_2O (c) formation and on the selectivity of NO reduction to nitrogen (d) at three different fixed catalyst potentials. $T = 580$ K, $P_{NO} = 0.75$ kPa.

of formation of CO_2 and N_2 and a decrease in the rate of formation of N_2O, resulting in the increase in the nitrogen selectivity shown in Figure 7d. Figure 7a also shows that at high sodium loadings, high values of P_{CO} cause an overall decrease in the rate of formation of CO_2, in agreement with the results illustrated in Figure 8a, as discussed below. Figure 7d shows that the nitrogen selectivity passes through a shallow maximum as P_{CO} increases and that this effect becomes more pronounced as Na coverage increases.

Figure 8a−d shows corresponding results for the dependence of the rates of production of CO_2, N_2, and N_2O and the nitrogen selectivity on P_{NO} at fixed P_{CO} for three different values of catalyst potential. No rate maxima are observed within the accessible P_{NO} range. These results show that at lower partial pressures of NO, the N_2 and CO_2 reaction rates exhibit maxima as the sodium loading is increased (rate(highest Na) < rate-(clean) < rate(moderate Na)). Figure 8d shows that the nitrogen selectivity is relatively insensitive to P_{NO}, other than at the highest Na coverage; in every case, there is a very small overall decrease in selectivity, in accord with the results of Belton et al.[20] Note also that the nitrogen selectivity of the unpromoted Rh film is 24%—a value that is fully consistent with those reported by Belton et al.[3] for the same reactant partial pressures and temperature, i.e., 40% over Rh(110), 26% over Rh(100), and 24% over Rh(111). Taken together, Figures 7d and 8d illustrate the point that over the entire range of partial pressures explored, Na acts to increase selectivity.

4. Discussion

4.1. Relationship between ΔV_{WR} and $\Delta\phi$. The relationship between the change in the ohmic-drop free potential difference between the working and reference electrodes (ΔV_{WR}) and $\Delta\phi$ deserves discussion. On one hand, Vayenas et al.[21] have derived the following expression:

$$e\Delta V_{WR} = \Delta\phi \tag{4}$$

and have validated it experimentally.[22] On the other hand, Zipprich et al.[23] have observed deviations from this equality, while Emery et al.[24] and Williams et al.[10] have failed to observed this equality. Most recently, for yttria-stabilized zirconia (an oxygen ion conductor), Vayenas et al.[25] have also observed deviations from eq 3, while Poppe et al.[26] found, for their samples, no variation of $\Delta\phi$ at all with ΔV_{WR}. Metcalfe and co-workers have investigated these discrepancies.[27,28] They showed that for any change in catalyst potential

$$e\Delta V_{WR} = \Delta\phi + e\Delta\Psi \tag{5}$$

where $\Delta\Psi$ is the change in outer (Volta) potential. They argued that eq 5 is valid when there is significant loss of spillover species from the surface, either by desorption or reaction. Equation 4 was taken to correspond to the case where there is true thermodynamic equilibrium between the promoter species in the electrolyte and those spilt over onto the metal catalyst surface. Thus, the relative rates of spillover to the catalyst and removal from the catalyst of the promoter species define two limiting cases. If the kinetics of electrochemical supply are fast whereas the rate of the loss of spillover species from the surface is relatively slow, then $e\Delta V_{WR} = \Delta\phi$. Conversely, if the electrochemical process is slow and the rate of the loss of spillover surface species is fast, then $e\Delta V_{WR} = \Delta\Psi$, since the coverage of spillover species will be negligible and will not

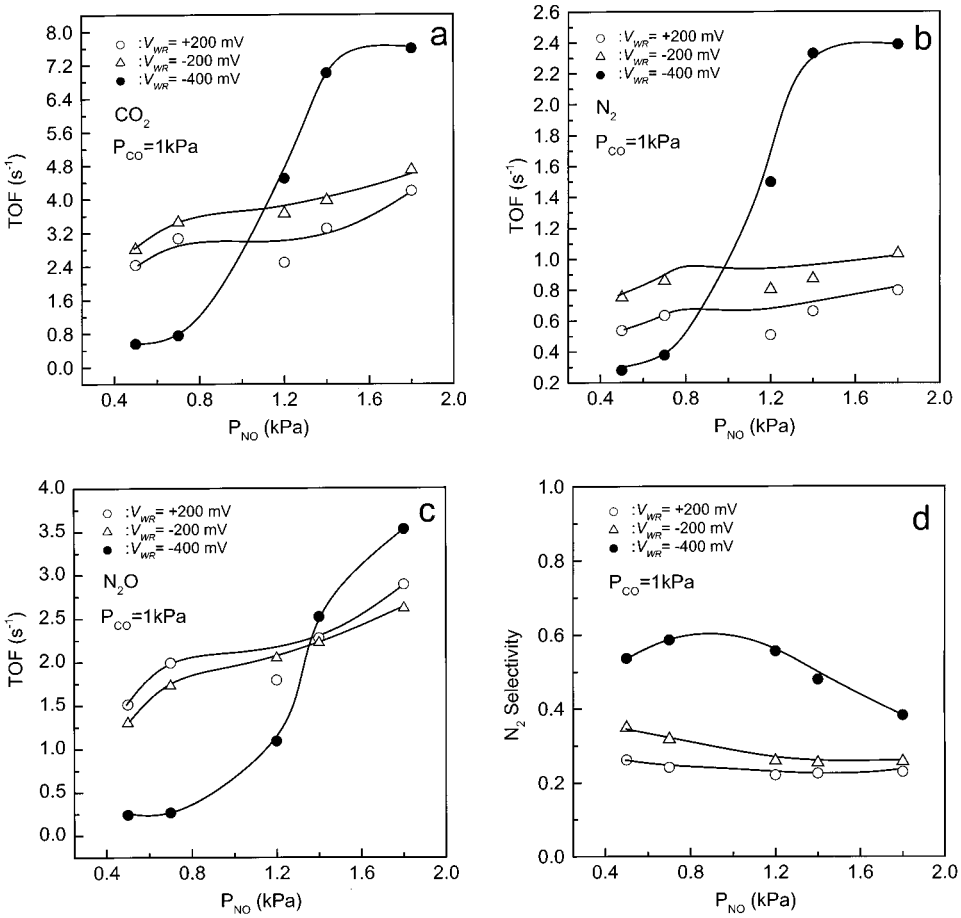

Figure 8. Effect of the partial pressure of NO (P_{NO}) on the rates of CO_2 (a), N_2 (b), and N_2O (c) formation and on the selectivity of NO reduction to nitrogen (d) at three different fixed catalyst potentials. $T = 580$ K, $P_{CO} = 1$ kPa.

appreciably modify the metal surface work function. Thus, eq 5 may be thought to describe the behavior in the general case, while eq 4 describes a limiting case.

Equation 4 predicts that a plot of $\Delta\phi$ against ΔV_{WR} should be linear with a slope of unity. Figure 5 shows that the relationship is indeed linear, but the slope is 0.32. Equation 4 also predicts a change in ϕ of -2 eV over the range of V_{WR} explored, corresponding to a maximum Na coverage of $\sim$0.08 ML.[13] In fact, the observed work function decrease was -0.65 eV, corresponding to $\vartheta_{Na} \approx 0.025$ ML.

A finite steady-state desorption rate for Na from the Rh surface could provide an explanation for these deviations from eq 4. However, at very low alkali coverages and under vacuum conditions, such as those used here, Na desorption from transition metal surfaces commences at $\sim$800 K (Pt{111},[29] Ru{001}[30]) or $\sim$700 K (Cu{111},[31] Ni{111}[32]). Although there is no reported value for the saturation coverage of Na on Rh{111} at 580 K, data for closely related systems indicate that it is highly unlikely that significant desorption occurs at 580 K for $\vartheta_{Na} \approx 0.025$ ML.[33] Thus, the evidence indicates that Metcalfe's model fails to provide an explanation for the observed deviation from eq 4.

Partial incorporation of Na adatoms into the Rh could provide an explanation for the deviation of the observed slope of the $\Delta\phi$ versus ΔV_{WR} plot from unity. If this were to occur, the work function change induced by a given amount of Na would be smaller than that induced by the same number of Na atoms on top of the Rh. This seems a likely possibility, given the findings of Lehmann et al.[34] These authors obtained results that strongly suggest subsurface incorporation of Na and K adatoms into Pt{111} under UHV conditions at low alkali coverages and at temperatures as low as 100 K. Note that although this effect could provide a plausible explanation for our results obtained under vacuum conditions, it is far from clear whether it is relevant to the behavior of an EP catalyst under operating conditions in the presence of a reactive gas atmosphere where the alkali is present as a surface compound. The results of Vayenas et al. and Metcalfe et al. were of course obtained at atmospheric pressure.

4.2. Reaction Mechanism. Our results are fully consistent with the view, advanced previously in regard to Pt-catalyzed NO reduction,[5,35] that Na acts to promote the rate-limiting step and that this step is the dissociation of adsorbed NO. In the specific case of the Rh-catalyzed NO + CO reaction, the identity of the rate-limiting step has been a matter of some controversy. The salient points are therefore considered here.

Belton et al.[3,20,36−38] carried out a series of detailed investigations in which they used Rh single-crystal surfaces as model catalysts, operated at atmospheric pressure. They concluded that at high N coverages, nitrogen desorption is not rate-limiting, as previously proposed.[36] It was also shown that the NO dissociation rate decreases with increasing coverage[20] and that NO and N react to form only N_2O and not N_2.[37] At moderate pressures, N_2 formation was accompanied by N_2O formation, and there was no evidence that N_2O readsorption played a significant role.[38] They showed that the reaction is structure sensitive, with the rates increasing as the metal surface atom density decreased in the order of (111) < (100) < (110)[3].

On the other hand, studies performed under UHV conditions[39] led to the conclusion that N atom recombination was the rate-

determining step. A comparison of these UHV results with the atmospheric pressure data of Belton et al. suggests that the relative contribution of the different elementary steps changes between the two pressure regimes. (Recall that no N_2O is produced under UHV conditions, whereas it is the main nitrogen-containing product at atmospheric pressures). This may be understood as follows. The NO dissociation rate is strongly dependent on NO coverage (due to the effects of lateral interactions and the availability of free sites). Under UHV conditions, the steady-state coverage is low, NO dissociation is extensive, the probability of the N + NO reaction is therefore small (no N_2O is observed), and the N recombination step is rate-limiting. This situation is reversed under atmospheric pressure conditions: now, the steady-state NO coverage is much higher, NO dissociation therefore becomes rate-limiting, and, as a result, N_2O formation can occur.

Given that that the partial pressures and temperature conditions employed in our experiments are very similar to the those used by Belton et al., it is reasonable to propose that the same mechanism prevails in the present case, i.e., that NO dissociation is rate-limiting.

In the discussion that follows, the term "sodium coverage" is used. This does not imply that the promoter phase is thought to be present in the form of chemisorbed metallic sodium under reaction conditions. Decreasing the value of the catalyst potential under UHV conditions does indeed pump chemisorbed metallic sodium to the Rh surface, as we have shown (Figures 3 and 5). As would be expected and as we have demonstrated previously,[35] this electrochemically supplied sodium is in the same chemical state as sodium deposited by vacuum evaporation. However, in the presence of a reactive atmosphere, one expects the Na to be present as a surface compound whose identity depends on the composition of the ambient gas. This too has been demonstrated previously. In the case of the EP of Pt-catalyzed NO reduction by propene, XPS shows that alkali nitrite and/or nitrate are present;[35,40] in the case of propene combustion, XANES shows that the promoter phase consists of alkali carbonate.[41]

4.3. Mechanism of Promotion. All our results may be understood in terms of the promotion of NO dissociation induced by electropumped Na. Our XPS data demonstrate directly the occurrence of this reversible spillover/backspillover effect, which correlates very well with the reversible response of the catalytic system. The dissociation of adsorbed diatomic molecules in the electric field of adjacent alkali cations has received a detailed theoretical analysis.[42] The field lowers the energy of the NO antibonding orbital with respect to the Fermi level. This increases charge transfer from the metal to the NO π^* orbital, increasing the strength of the metal−N bond and decreasing the strength of the N−O bond. In the specific case of Rh/NO, studies on Rh(111)/K[43,44] and Rh(100)/Na[45] reveal the expected strengthening the metal−N bond and weakening of the N−O bond: both effects act to increase activity and selectivity.

The following reaction mechanism permits a rationalization of the EP by Na of the Rh-catalyzed NO + CO reaction

$$CO(g) + S \rightarrow CO(a) \quad (6)$$

$$\mathbf{NO(g) + S \rightarrow NO(a)} \quad \text{promoted by Na} \quad (7)$$

$$\mathbf{NO(a) + S \rightarrow N(a) + O(a)} \quad \text{promoted by Na} \quad (8)$$

$$CO(a) + O(a) \rightarrow CO_2(g) + 2S \quad (9)$$

$$NO(a) + N(a) \rightarrow N_2O(g) + 2S \quad \text{inhibited by Na} \quad (10)$$

$$N(a) + N(a) \rightarrow N_2(g) + 2S \quad (11)$$

where S represents a vacant site for adsorption. It was previously proposed by Belton et al.[3] in regard to catalysis by Rh, by Lambert and Comrie[1] in regard to the CO + NO reaction over Pt, and by ourselves in regard to the EP of the Pt-catalyzed reaction.[5] The adsorption and dissociation of the reactants depend on the availability of such free sites (reactions 6−8). In this scheme, eq 8 is rate-limiting, both eq 7 and eq 8 are enhanced by Na, and nitrogen selectivity depends on the relative rates of reactions 10 and 11. On this basis, Na promotes activity and nitrogen selectivity as a result of accelerating the key reaction-initiating step (eq 8). This leads to an increase in the coverage of N(a) and O(a) and a decrease in that of NO(a). As a consequence, there is an increase in the rates of steps 9 and 11 and a decrease in the rate of step 10, yielding the observed increase in overall activity and nitrogen selectivity (Figure 6). Additionally, the kinetic data (Figure 7) demonstrate the beneficial effect of Na in increasing the adsorption strength of NO relative to CO such that higher CO partial pressures are required before CO poisoning sets in.

Figure 7d shows that the nitrogen selectivity exhibits a maximum as a function of P_{CO} for fixed P_{NO}. This may be understood as follows. Dissociation of NO(a) requires a nearest-neighbor vacant site; therefore, nitrogen selectivity is expected to increase with the number of such sites. When P_{CO} is low, the surface will be mainly covered by O atoms, inhibiting NO dissociation; as P_{CO} increases, the coverage of O decreases due to formation of CO_2, freeing up sites for NO dissociation. Thus, N_2 selectivity increases with P_{CO}. When P_{CO} is sufficiently high, N_2 selectivity eventually decreases because site blocking by CO begins to inhibit NO dissociation. Therefore, the nitrogen selectivity passes through a maximum. The effect is more pronounced at higher sodium coverages as a result of the enhanced NO dissociation induced by Na.

As noted previously, Figure 8a,b shows that the reaction rates exhibit a maximum as the sodium loading is increased for low NO partial pressures at a fixed CO partial pressure. This observation is consistent with the result displayed in Figure 7a, namely, that at the highest CO:NO ratio, rate(highest Na) < rate(clean) < rate(moderate Na). This may reflect the site blocking effect of islands of Na−CO surface complexes[46] that are known to be stable under these conditions. At sufficiently low CO:NO ratios, there is a switch in behavior: the activity now increases with Na coverage. This may be rationalized in terms of increased coverage by NO and its dissociation products, especially O(a), which act to inhibit Na−CO complex formation and, hence, concomitant poisoning.

As noted earlier, reaction rates over the unpromoted catalyst exhibit maxima as a function of CO partial pressure (Figure 7) and are approximately independent of NO partial pressure (Figure 8). Such behavior was observed for the NO + CO reaction over Pt;[5] it is also in good agreement with the results of Hendershot and Hansen,[47] who studied the CO + NO reaction over Rh(100). Belton et al.[19] reported zero order in both CO and NO under conditions similar to those used in this study. However, close inspection of the data reveals no significant divergence between their findings and ours. Thus, if we plot the results presented in Figures 7 and 8 logarithmically, in the manner employed in ref 19, it becomes apparent that our data are in very good agreement with those of Belton et al.; the variation of the unpromoted reaction rates with reactant partial pressures is rather small in the range of partial pressures studied.

The EP by Na of the Rh-catalyzed CO + NO reaction exhibits both similarities and differences compared with the EP of the Pt-catalyzed reaction.[5] In both cases, increasing the sodium

coverage causes an increase in the rates of formation of CO_2 and N_2 and results in a pronounced increase in the nitrogen selectivity. However, in the case of Pt, increasing the sodium coverage causes the rate of formation of N_2O to go through a maximum, whereas in the present case, under similar conditions, the N_2O rate always decreases with increasing Na loading. This reflects the fact that clean Rh surfaces are more efficient than clean Pt surfaces at dissociating NO. For example, NO dissociates on Rh(111) at low ϑ_{NO} (<0.25),[48,49] whereas it does not dissociate on Pt(111) under the same conditions.[1,50]

5. Conclusions

1. The coverage of electropumped Na on a thin-film Rh catalyst contacted with a sodium-ion-conducting solid electrolyte is determined by the catalyst potential; the effect is fully reversible.

2. The Na coverage and the Rh work function scale linearly with the catalyst potential. The sodium coverage varies from 0 to ~0.02 monolayers—the range over which the catalytic performance also improves dramatically.

3. The CO + NO reaction exhibits strong, reversible electrochemical promotion under Na pumping to the rhodium catalyst. This is due to the in situ control of sodium coverage over the catalyst surface. Activity and selectivity toward N_2 formation are markedly improved by a factor of 3 and from 24% to 80%, respectively.

4. NO promotion is due to (i) the enhanced NO versus CO chemisorption and (ii) the Na-induced dissociation of chemisorbed NO. The latter factor is primarily responsible for the Na-induced increase in nitrogen selectivity.

Acknowledgment. We thank Norman Macleod for his assistance with the surface area determination. F.J.W. acknowledges financial support from Fundación YPF, Fundación Antorchas, British Council Argentina, and King's College Cambridge. This work was supported by the U.K. Engineering and Physical Sciences Research Council and by the European Union under Grants GR/M76706 and BRPR-CT97-0460, respectively.

References and Notes

(1) Lambert, R. M.; Comrie, C. M. *Surf. Sci.* **1974**, *46*, 61.
(2) Zaera, F.; Gopinath, C. S. *J. Chem. Phys.* **1999**, *111*, 8088.
(3) Herman, G. S.; Peden C. H. F.; Schmieg, S. J.; Belton, D. N. *Catal. Lett.* **1999**, *62*, 131 and references therein.
(4) Taylor, K. C. *Catal. Rev. Sci. Eng.* **1993**, *35*, 457.
(5) Palermo, A.; Lambert, R. M.; Harkness, I. R.; Marina, O.; Vayenas, C. G. *J. Catal.* **1996**, *161*, 471.
(6) Williams, F. J.; Aldao, C. M.; Palermo, A.; Lambert, R. M. *Surf. Sci.* **1998**, *412/413*, 174.
(7) Yentekakis, I. V.; Lambert, R. M.; Tikhov, M. S.; Konsolakis, M.; Kiousis, V. *J. Catal.* **1998**, *176*, 82.
(8) Konosolakis, M.; Nalbantian, L.; MacLeod, N.; Yentekakis I. V.; Lambert, R. M. *Appl. Catal., B* **1999**, *22*, 123.
(9) Konsolakis, M.; Macleod, N.; Isaac, J.; Yentekakis, I. V.; Lambert, R. M. *J. Catal.*, in press.
(10) Williams, F. J.; Palermo, A.; Tikhov, M. S.; Lambert, R. M. *J. Phys. Chem B.* **2000**, *104*, 615.
(11) Komai, S.; Hattori, T.; Murakami, Y. *J. Catal.* **1989**, *120*, 370.
(12) Ladas, S.; Bebelis, S.; Vayenas, C. G. *Surf. Sci.* **1991**, *251/252*, 1062.
(13) Mate, C. M.; Kao, C. T.; Somorjai, G. A. *Surf. Sci.* **1988**, *206*, 145.
(14) Carley, A. F.; Roberts, M. W. *Proc. R. Soc. London, Ser. A* **1978**, *363*, 403.
(15) Yeh, J. J.; Lindau, I. *At. Data Nucl. Data Tables* **1985**, *32*, 1.
(16) Penn, D. R. *J. Electron. Spectrosc. Relat. Phenom.* **1976**, *9*, 29.
(17) Verhoef, R. W.; Asscher, M. *Surf. Sci.* **1997**, *391*, 11.
(18) Permana, H.; Ng, K. Y. S.; Peden, C. H. F.; Schmieg, S. J.; Lambert, D. K.; Belton, D. N. *J. Catal.* **1996**, *164*, 194.
(19) Permana, H.; Ng, K. Y. S.; Peden, C. H. F.; Schmieg, S. J.; Belton, D. N. *J. Phys. Chem.* **1995**, *99*, 16344.
(20) Peden C. H. F.; Belton, D. N.; Schmieg, S. J. *J. Catal.* **1995**, *155*, 204.
(21) Vayenas, C. G.; Bebelis, S.; Lintz, H. G. *Catal. Today* **1992**, *11*, 303.
(22) Vayenas, C. G.; Bebelis, S.; Ladas, S. *Nature* **1990**, *343*, 625.
(23) Zipprich, W.; Wiemhofer, H. D.; Vohrer, U.; Gopel, W. *Ber. Bunsen-Ges. Phys. Chem.* **1995**, *99*, 1406.
(24) Emery, D. A.; Middleton, P. H.; Metcalfe, I. S. *Surf. Sci.* **1998**, *405*, 308.
(25) Tsiplakides, D.; Neophytides, S.; Vayenas, C. G. *Solid State Ionics*, in press.
(26) . Poppe, J.; Volkening, S.; Schaak, A.; Schutz, E.; Janek, J.; Imbihl, R. *Phys. Chem. Chem. Phys.* **1999**, *1*, 5241.
(27) Emery, D. A.; Middleton, P. H.; Metcalfe, I. S. *J. Electrochem. Soc.* **1999**, *146*, 2188.
(28) Emery, D. A.; Middleton, P. H.; Metcalfe, I. S. *J. Electrochem. Soc.* **1999**, *146*, 2194.
(29) Harkness, I. R. Ph.D. Thesis, University of Cambridge, Cambridge, U.K., 1994.
(30) Doering, D. L.; Semancik, S. *Surf. Sci.* **1983**, *129*, 177.
(31) Tang, D.; McIlroy, D.; Shi, X.; Su, C.; Heskett, D. *Surf. Sci.* **1991**, *225*, L497.
(32) Gerlach, R. L.; Rhodin, T. N. *Surf. Sci.* **1970**, *19*, 403.
(33) Diehl, R. D.; McGrath, R. *Surf. Sci. Rep.* **1996**, *23*, 43.
(34) Lehmann, J.; Roos, P.; Bertel, E. *Phys. Rev. B* **1996**, *54*, R2347.
(35) Yentekakis, I. V.; Palermo, A.; Filkin, N. C.; Tikhov, M. S.; Lambert, R. M. *J. Phys. Chem. B* **1997**, *101*, 3759.
(36) Belton, D. N.; DiMaggio, C. L.; Ng, K. Y. S. *J. Catal.* **1993**, *144*, 273.
(37) Belton, D. N.; DiMaggio, C. L.; Shmieg, S. J.; Ng, K. Y. S. *J. Catal.* **1995**, *157*, 559.
(38) Ng, K. Y. S.; Belton, D. N.; Shmieg, S. J.; Fisher, G. B. *J. Catal.* **1994**, *146*, 394.
(39) Gopinath, C. S.; Zaera, F. *J. Catal.* **1999**, *186*, 387.
(40) Williams, F. J.; Palermo, A.; Tikhov, M. S.; Lambert, R. M. *J. Phys. Chem. B* **1999**, *103*, 9960.
(41) Filkin, N. C.; Tikhov, M. S.; Palermo, A.; Lambert, R. M. *J. Phys. Chem. A* **1999**, *103*, 2680.
(42) Lang, N. D.; Holloway, S.; Norskov, J. K. *Surf. Sci.* **1985**, *150*, 24.
(43) Bugyi, L.; Solymosi, F. *Surf. Sci.* **1987**, *188*, 475.
(44) Bugyi, L.; Kiss, J.; Revesz, K.; Solymosi, F. *Surf. Sci.* **1990**, *233*, 1.
(45) Hochst, H.; Colavita, E. *J. Vac. Sci. Technol., A* **1986**, *4*, 1442.
(46) Bertolini, J. C.; Delichere, P.; Massardier, J. *Surf. Sci.* **1985**, *160*, 531.
(47) Hendershot, R. E.; Hansen, R. S. *J. Catal.* **1986**, *98*, 150.
(48) Borg, H. J.; Reijerse, F. C. J. M.; van Santen, R. A.; Niemantsverdriet, J. W. *J. Chem. Phys.* **1994**, *101*, 10052.
(49) Hopstaken, M. J. P.; van Gennip, W. J. H.; Niemantsverdriet, J. W. *Surf. Sci.* **1999**, *69−73*, 433.
(50) Comrie, C. M.; Weinberg, W. H.; Lambert, R. M. *Surf. Sci.* **1976**, *57*, 619.